Proceedings of ASME Turbo Expo 2011
GT2011
June 6-10, 2011, Vancouver, British Columbia, Canada

GT2011-46368

A CORRELATION BETWEEN VIBRATION STRESSES AND FLOW FEATURES OF STEAM TURBINE LONG BLADES IN LOW LOAD CONDITIONS

Naoki Shibukawa, Tomohiro Tejima,
Power and Industrial Systems Research and Development Center
Toshiba Corporation
Yokohama 230-0045, Japan
Email: naoki.shibukawa@toshiba.co.jp

Yoshifumi Iwasaki, Itaru Murakami, Ikuo Saito
Keihin Product Operations, Toshiba Corporation
Yokohama 230-0045, Japan

ABSTRACT

The vibration stress of long steam turbine blades during low load operating conditions is examined in this paper. A series of experiments has been carried out to investigate the vibration stress behavior, and the steady and unsteady pressure fluctuation. It is found that a steady pressure distribution over the blade tip is much to do with the unsteady pressure and fluctuation of the vibration stress. A precise investigation of unsteady wall pressure near blade tip explains the relationship between pressure fluctuation and the vibration stress, and reveals the existence of particular frequency which affects blade axial modes.

Blade to blade flow mechanisms and aerodynamic force and properties during low load operating condition were investigated by a steady CFD simulation. FFT of aerodynamic force by another steady full arc CFD simulation provides various pattern of harmonic excitation which account for the behavior of vibration stresses well. The mechanism of the rapid stress increase and a step drop were examined by considering CFD results and measured unsteady pressure data together.

INTRODUCTION

It is generally recognized that the vibration stress of long steam turbine blades may increase when a turbine experiences low load conditions, such as initial loading points or high back pressure operations. Manufacturers must work within operational limits to avoid problems with the blades, which may sometimes cause a mismatch with customer requirements and can be a negative factor in otherwise successful contracts. In the case of nuclear turbines, it is clear that reliability must be paramount and therefore the risk of blade accidents occurring must be kept as low as possible. According to the policy that safety is the most important issue, steam turbines are often designed with substantial structural margins, which are apt to decrease thermal efficiencies.

Research into the reliability of steam turbine long blades progressed significantly in the 1980's, when large size last stage blades were required as one of the main technologies of high efficiency steam turbines. Avoiding resonance during full load operation is of primary importance in the design process On the other hand, keeping the blade away from low load critical conditions has been the only way to avoid destructive random vibrations. Although the latter has been recognized as an operational matter, many studies have been carried out to understand the flow aspects and mechanism of the related increasing vibration stress. Ikeuchi et al. [1] focused on flutter and found the limits in conditions where it occurs experimentally. Iwanaga et al. [2] explained a huge reverse flow into a blade row and associated fluid buffeting as an excitation promoter. They additionally theoretically constructed a reverse flow loss model which could predict the stress increase point. They also conducted useful experimental work and many researchers agree with their basic ideas. Suzuki et al. [3] and Mujezinovic et al. [4] reported on a newly developed last stage blade with successfully validated results. Iwanaga et al. [2] and Sugita et al. [5] performed vibration stress measurements in actual steam turbines. In accordance with the computer performance enhancement, CFD and advanced structure analysis was effectively applied to predict the behavior of vibration stresses. Stüer et al.[6] investigated the interaction between nozzle wakes and blade shock waves by unsteady CFD, which did not directly deal with low load conditions but produced unsteady analysis that will be useful in the near future. Masuzawa et al. [7] developed a quasi 3D fluid analysis code with a modified FLIC (Fluid-in-Cell) method, in which model turbine test data were taken to improve the prediction performance. As for a structural approach, Saito et al. [8] adopted a multi-degree of freedom spectrum analysis to simulate random vibration mechanisms and obtained good agreement with experimental data. Nakamura et al. [9] reported a multi-stage quasi-3D unsteady analysis that was applied to predict a flow aspect in a nuclear turbine and which showed that the reverse region could be extended upstream to the L-2 stage. Segawa [10] conducted detailed unsteady pressure measurements in a steam turbine model test facility to obtain a peak of pressure fluctuations, which could be assumed to correspond with the vibration stress trend. Truckenmüller et al.[11] measured unsteady pressure field in a model turbine and blade stress simultaneously during windage. Gerschütz et al.[12] extended the research to organize the correlative feature, and obtain the rotating instability in turbine. Sigg et al.[13] performed numerical study for the windage condition and the results achieved good agreement with experiments.

Although previous research has provided very useful results, there is still remaining issue to be investigated. This paper presents a correlation between vibration stress behaviors and flow features using experimental results from a series of model turbine tests. It also explains the possible flow mechanism in low load operating conditions and suggests a set of vibration stress prediction methods.

NOMENCLATURE

κ	ratio of specific heat
ρ	density
v	velocity
v_{rel}	relative inlet velocity for a blade
σ_{vib}	vibration stress
σ_{bend}	bending stress
Tr	torque at local height
T	temperature
Cp	specific heat at constant pressure
h	local height
H	total height
r	radius
dh	height increment
dr	radial increment
dA	annulus area increment
Z	section modulus of a blade
Vax	axial flow velocity
PS	pressure side
SS	suction side
L.E.	leading edge
T.E.	trailing edge
OA	overall
FFT	fast Fourier transform
B.P.	back pressure
PRtip	pressure ratio over L-0 blade
L-0,1,2	last stage, 1, 2 stage upstream

2 EXPERIMENTAL STUDY

Experimental Facility

A typical last stage of a large size nuclear plant was chosen to be investigated. Both aerodynamic and mechanical measurements of the stage were performed in an experimental low-pressure model turbine. A schematic diagram of the 10 MW model steam turbine facility used in the current study is shown in Figure 1. The model turbine stage assembly used in the present study is shown in Figure 2. As shown in Figure 1, the boiler provides superheated steam to the model turbine through a conversion valve that controls both the steam pressure and temperature. Since the superheated steam does work and expands through the model turbine stages to the wet steam region, model turbine steam conditions are very close to those in actual full-scale steam turbines. The turbine shaft is split between the upstream stages and the last stage. As quite low load and high exhaust pressure conditions were required in the test program, the last stage rotor was coupled with a drive turbine, which can control the rotational speed with sufficient precision. Table 1 shows the model turbine's last stage features. Six L-0 blades make a group, each of which is tied by loose type wires in the same way as in the actual machine. The model turbine rotates at 6300 rpm to keep the velocity triangles in the inlet and exit planes of the nozzle and blade the same as in the full-scale steam turbines. In the measurement system, the operational data of the rig are automatically and continuously accumulated into a set of data loggers. The turbine inlet temperature, pressure, exhaust pressure and condensed water volume flow rates are measured as the principal data to specify the operating condition. Torque and rotational speed data are also important in order to know the steam condition of the turbine.

Test Conditions

The L-0 exit average axial flow velocity (Vax) is one of the popular parameters to estimate the last stage loading or performance. Usually it is calculated with a mass flow rate per unit area and the specific volume can be calculated using the measured data described above. However, at very low load conditions, where the flow around the last stage contains a strong reverse region and the exhausted steam is heated up to dry zone by a windage, the averaged annulus velocities have to be taken as one of the blade loading indicators. In this study, most of the test cases were carried out in dry exhaust conditions. Figure 3 describes the test conditions on a vacuum - mass flow chart. Two series of the test were planned, one of which was done at relatively low exhaust pressure, which is the nominal operating condition, and the other at pressure about twice as high as the lower cases. The Vax range of the test cases was from 12m/s to 70m/s approximately with variation bands as shown in Figure 3. Although the test conditions were set based on time-averaged data, the mass flow rate fluctuates during measurement because it corresponds to the governor control. Also, the measurement error for the exhaust pressure is estimated ±0.2 kPa. A full speed case with no mass flow was conducted to identify the vibration stress in a no load condition, at which only the last stage rotor was driven by the drive turbine.

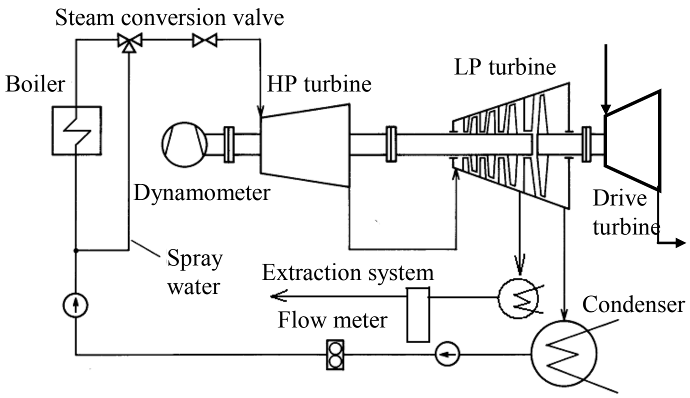

Figure 1 Model steam turbine system

Table 1 Model turbine last stage features

Main Features of the test model		
Rotational Speed	[rpm]	6300
Blade Height	[mm]	314.5
Annulus Area	[m2]	0.95
Tip Speed	[m/s]	421
Boss ratio(tip/hub)		2.05
Fastening		Finger
Connection Type		
Tip		Loose Wire
Mid Span		Loose Wire

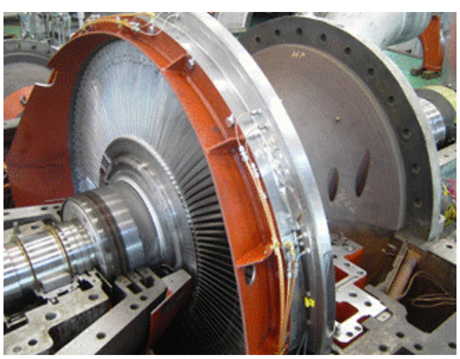

Figure 2 Model turbine L-0 blades

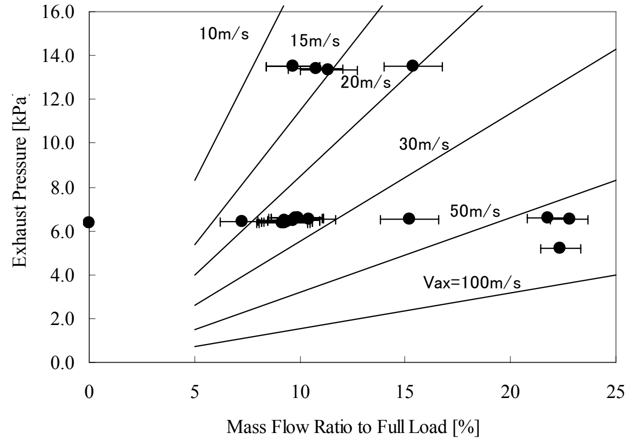

Figure 3 Low load test conditions

<u>Measurement Instruments</u>

In the present study, both aerodynamic and mechanical measurements were taken. For the steam flow, wall pressure was precisely measured. No traverse probe was installed for fear that the probe head and stem would seriously affect the flow pattern in such a low load condition. Figure 4 shows a pneumatic pressure tap and unsteady pressure sensor for the L-0 nozzle. Even though the main object is the last stage, pressure taps and sensors were also arranged at upstream stages, as shown in Figure 5. The accuracy of the pneumatic sensor is 0.2% of the full-scale range which will be equivalent to about 4% of Vax value, which is small enough to classify each test condition. A group of Kulite's silicon diaphragm pressure transducers "XCEL-100" were mounted on the outer end wall of the stator to investigate unsteady pressure variation, which is expected to correlate with the vibration stress of the blades.

In the measuring system, the vibration stress is obtained from a strain gage mounted on the suction side of the L-0 blade, as shown Figure 6. The strain signal is transmitted by the FM telemetric system. Figure 7 shows a block diagram of the FM telemetric system. A FM transducer is mounted on the middle section of the rotor shaft. The signal is received by the receiving antenna mounted on the casing of the rotor shaft. This signal is analyzed by the FFT analyzer.

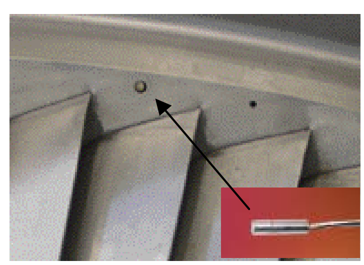

Figure 4 Pressure measurement tap and unsteady sensor

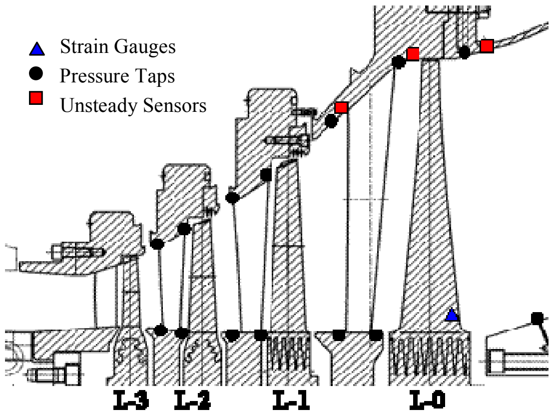

Figure 5 Measurement layout of the test turbine

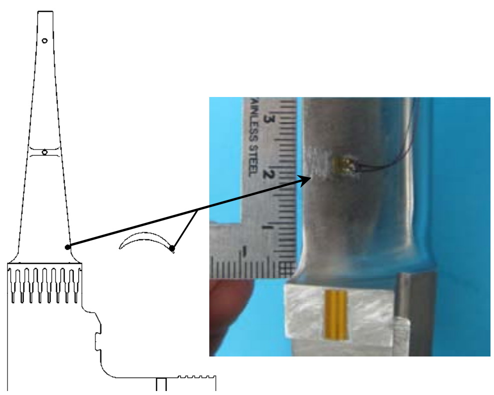
Figure 6 Strain gauge on the last stage blade

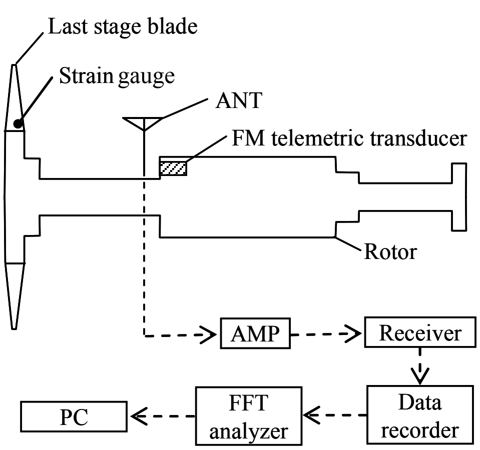

Figure 7 Block diagram of FM telemetric system

Experimental Results

Figure 8 shows the vibration stress against Vax. All stress plots are the overall (OA) values, those are, the summations of power spectrum of a frequency band between 0 to 1600Hz throughout the paper, which are normalized by the value of case 1 in this Figure. Case 1 represents the no steam flow condition, and case 2, case 3, case M, and case 4 represents 7, 9, 13, 20 per cent load condition, respectively. It can be seen that there are two groups of data, the lower back pressure group (about 6.5kPa), and the higher back pressure group (about 13.5kPa). For lower back pressure cases, the vibration stress tends to rise up to the peak when Vax goes down between 30 and 25 m/s, and with further Vax reduction, the vibration stress undergoes a steep drop. This is the same phenomena as the result of previous researches **[11] [12]**. As for the higher back pressure cases, although the examined Vax range is limited, it seems to be in the same manner as the lower back pressure case with regard to less than 25m/s condition. To compare the stress level of the two groups, with an assumption that the density is proportional to the back pressure, the higher back pressure vibration stresses were multiplied by the back pressure ratio (6.5/13.5) and plotted in Figure 8. As the corrected plots seem to belong to the lower back pressure group, it was confirmed that back pressure is one of the dominant parameters to determine vibration stress level. To investigate in detail, typical five test cases, those are case 1 to case 4 and case M, were selected as shown in Figure 8. It should be additionally mentioned that the design criteria in terms of the material strength is as about eighteen times large as that of case 1, which means considerable maximum vibration stress should be much lower than the criteria.

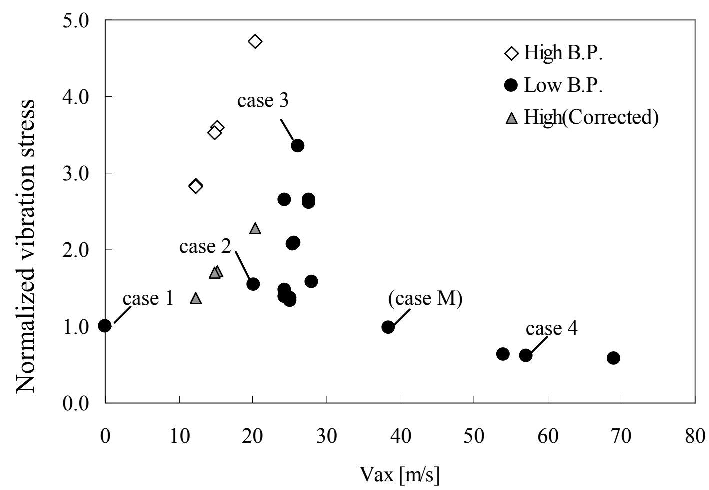

Figure 8 Vibration stress variation against L-0 Vax

Figure 9 shows the frequency spectrum analysis of the vibrating stress for each case. Each spectrum is normalized by the overall value of case 1. In terms of the harmonic number, the axial 1st mode of the blade is in between 4th and 5th, and axial 2nd mode is in 5th and 6th.

As for the case 2, it can be observed that the axial 1st mode and the tangential 1st mode are increased, and in the case 3, it is clearly shown that the axial 2nd mode gets much higher level. In the case 4, the vibration stress decreased in all modes, and the overall value goes down to a lower level. As the rotational speed was kept the same in all cases, the detuning ratio which influences vibration stress should be constant. Then, it can be considered that some aspects of aerodynamic force should be resonant with these axial vibration modes.

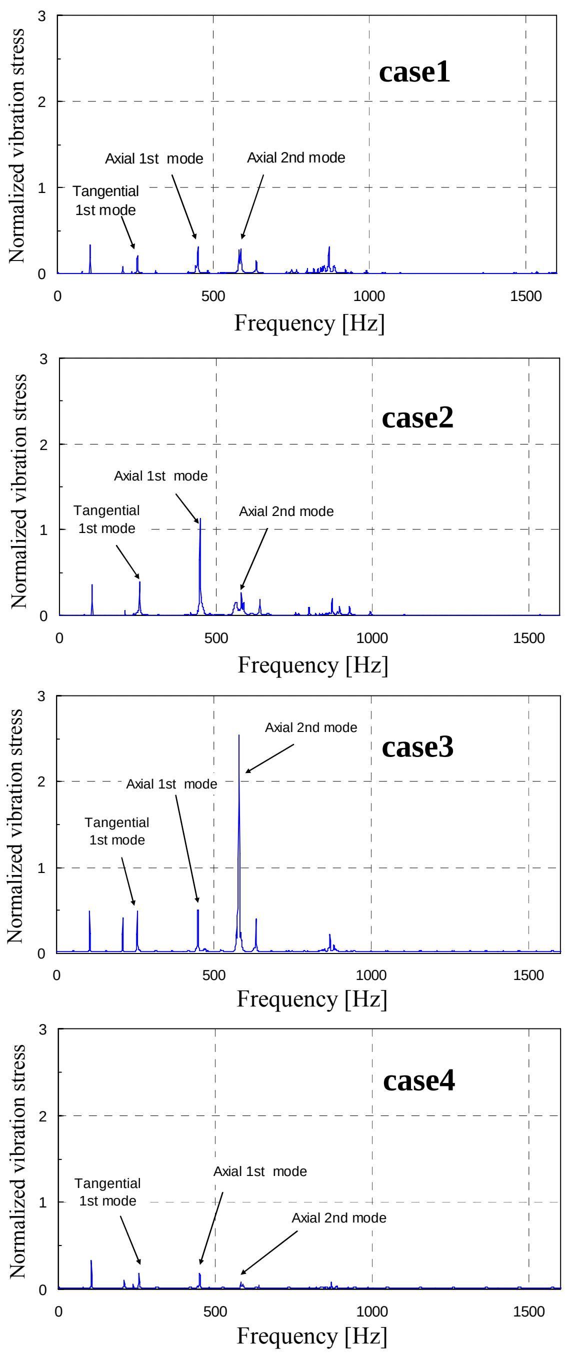

Figure 9 Frequency analyses of typical test cases

Time-averaged pressures

Although vibration stress is a phenomena related with unsteady fluid force, steady pressures taken by pneumatic measurements were firstly examined to find particular aerodynamic features which can be related to vibration stress levels. Figure 11 plots the end wall pressure distributions normalized by the L-0 exit pressure in each case. In case 4, the pressures go down from the inlet to the outlet and the steam moves smoothly. In cases 2 and 3 however, the exit pressures behind the L-0 blade are relatively higher than those of L-0 nozzle, so that reverse flow from the blade to the nozzle is likely to appear. The pressure trend of case 4 is so different from the others that it can be said that pressure distribution is one of the key items for vibration stress prediction.

According to a research by Gerschütz et al. **[12]**, the pressure ratio over the L-0 blade tip was investigated. Although there is a scattering, the pressure ratios can be seen to increase when Vax is reduced, as shown in Figure 12. At the condition of case 3, the pressure ratio exceeds 1.0, where the tip section of the blade possibly performs like a compressor and is likely to suffer from aerodynamic excitation **[12]**.

As for case 2, in spite of the pressure ratio of it is almost same, its vibration stress is much less than that of case 3. So, it still can not be sufficiently explained with the consideration above.

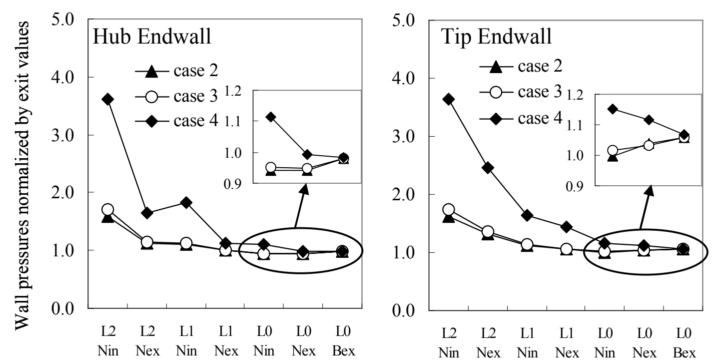

Figure 11 End wall pressure comparisons among the three low load cases

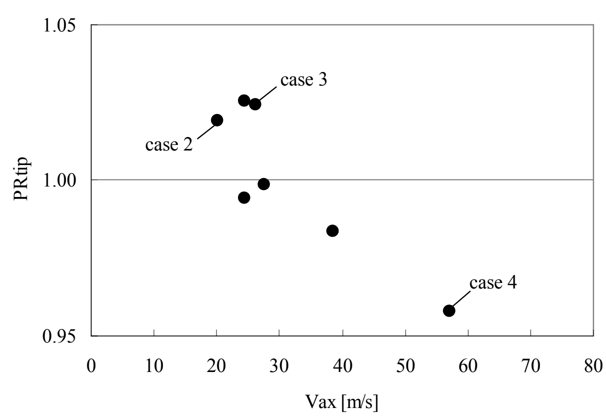

Figure 12 Pressure ratios over the L-0 blade tip (exit/inlet)

Unsteady pressure fluctuation

To understand more about the mechanism of vibration stress variation, the correlation between vibration stress and pressure fluctuation was investigated.

Figure 13 compares the overall values of unsteady pressure and the steady pressure at the tip end wall of case 2. It can be seen that the fluctuation level increases in the same manner as the steady pressure, which explains that the unsteady pressure measurement was properly performed. In the Figure, the unsteady pressures of L-0 nozzle inlet (Nin) and exit (Nex) for case 3 and case 4 were also plotted, which shows remarkable pressure variation at the nozzle exit among the three cases.

To find the relationship between the pressure variations, Figure 14 compares the overall values of nozzle exit tip end wall pressure fluctuation and blade vibration stresses, which are the summation of the power spectrum shown in Figure 9. Pressure fluctuation is highest at case 3, which traces approximately the same trend as vibration stress, but the order of the fluctuation is opposed to that of vibration stress in terms of case 2 and case 4.

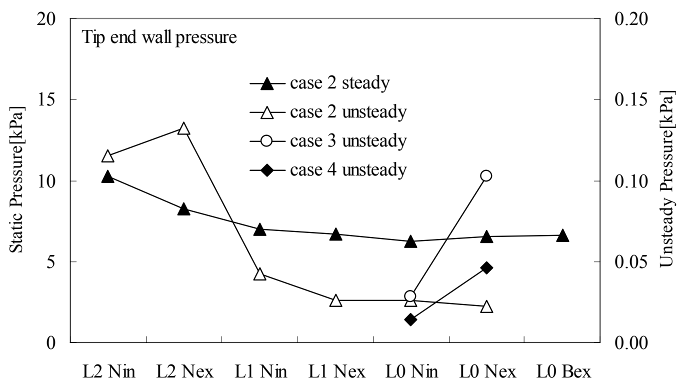

Figure 13 Steady and unsteady wall pressure of the last three stages

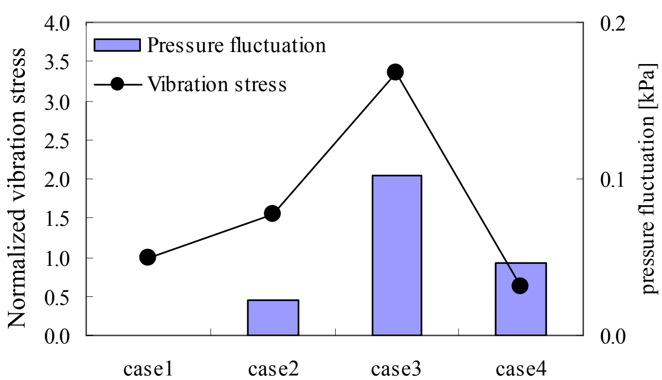

Figure 14 Pressure fluctuation and vibration stress
(all stress values are normalized by overall stress of case 1)

Figure 15 shows the result of spectrum analyses of unsteady pressure at the exit of the L-0 nozzle end wall of case 2, case 3 and case 4. It can be seen that case 3 shows higher amplitude in more than 1000Hz, and also indicates the strongest frequency of slightly less than 500Hz which is close to the axial 2nd mode. Even though it is not exactly the same as the natural frequency, this superior frequency and the higher level spectrum in 400 - 600Hz can be thought to encourage the resonance to axial 1st and 2nd mode.

As for case 4, higher level fluctuations are observed in between 200 - 400 Hz, and average value is apparently higher than that of case 2 which indicates quite low level fluctuation along the whole range, but the vibration stress is less than that of case 2 as mentioned above. As it seems difficult to find good reason for the inconsistency, there should be some other features of the flow, such as flow directions, thrust or bending force on the blade and their radial distribution.

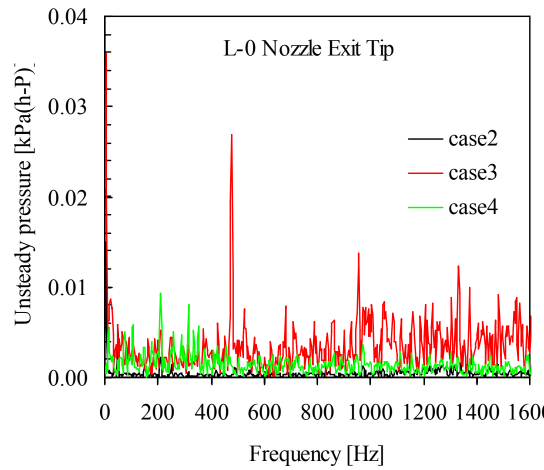

Figure 15 Wall pressure fluctuation at L-0 nozzle exit

CFD INVESTIGATIONS AND DISCUSSIONS

Computations

Although steady analysis is not available to investigate excitation aerodynamic force, it is thought to be attractive to use it as design tool with an assumption that amplitude of unsteady pressure has linearity with that of steady pressure. Then, several studies by two kinds of steady CFD simulation were carried out to find correlations between steady aerodynamic force and vibration stress. The first code was an in-house blade-to-blade FVM (Finite Volume Method) code, which was used rather like a throughflow analysis tool. A structured mesh with about 0.3 million points for four stages was used and the Baldwin-Lomax turbulence model is integrated into the code, which was assumed to be practical for various cases. In the present study, this code was used to examine detailed flow conditions for the last stage.

The other simulation used a STAR-CD V3.26 commercial software package, which was used for full arc, four stage analyses to investigate the interaction between the nozzles and the rotor blades. An unstructured mesh was used with almost 6.3 million points. The RNG k-ε turbulence model was selected. The computations were run in steady mode using the models for multiple rotating reference frames. With this option, although it is not unsteady analysis, rotor blades are distributed at several positions relative to the nozzles and will sense cyclic fluctuation. Figure 16 shows the computational mesh.

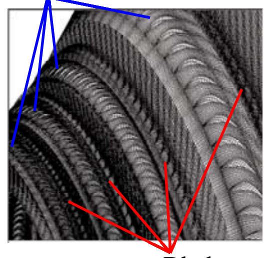

Figure 16 Computational mesh for full arc simulations

For both CFD analyses, experimental results were applied as boundary conditions, these being inlet total pressure and total temperature and the exit static pressure of the stage. In the final step of the analyses, the mass flow rates were adjusted to the measured data, prior to the inlet total pressure.

In the analyses, steam is treated as a perfect gas and its thermal property is provided by following equations,

$$\kappa = f(p, v) \tag{1}$$

$$Cp = \frac{\kappa}{\kappa - 1}\frac{p \cdot v}{T} \tag{2}$$

where,

p is estimated static pressure at a middle stage

v is estimated specific volume at a middle stage

<u>Four stage analyses</u>

To understand the flow aspect of each case, three dimensional blade-to-blade stage analyses were initially carried out. The flow mechanism of blade tip region during the low load condition was mainly examined. Figure 17 compares the circumferentially-averaged streamlines in each case. With Vax decreasing, same as many previous research[2][11][13], it can be seen that the reverse flow starts near the hub end wall of the blade exit and it grows to a large circulation as shown in case 4. Decreasing Vax more, in case M, another reverse flow occurs in front of the blade tip. Proceeding to case 3 and case 2, the circular flow at the tip grows and an unstable flow appears at hub region of nozzle inlet and grows larger.

A series of experimental data was applied for CFD and the results were validated as shown in Figure 18. Both series of plots are tip end wall pressure for each position, which shows good agreements.

In the beginning, the relationship between the estimated bending stress by CFD and the vibration stress was examined in order to attempt the fundamental idea that a blade is taken as a cantilever in a low speed flow. Computed dynamic pressures of each grid in the examined plane just before the blade were averaged and used for the fluid force calculation. Then, bending

stresses "σ_{bend}" shown in Equation (3) at the same position as the strain gauge were compared with measured stresses.

$$\sigma_{bend} = \left[\frac{1}{2}\int \rho \cdot v_{rel}{}^{2} dA \cdot hdh\right] / Z \tag{3}$$

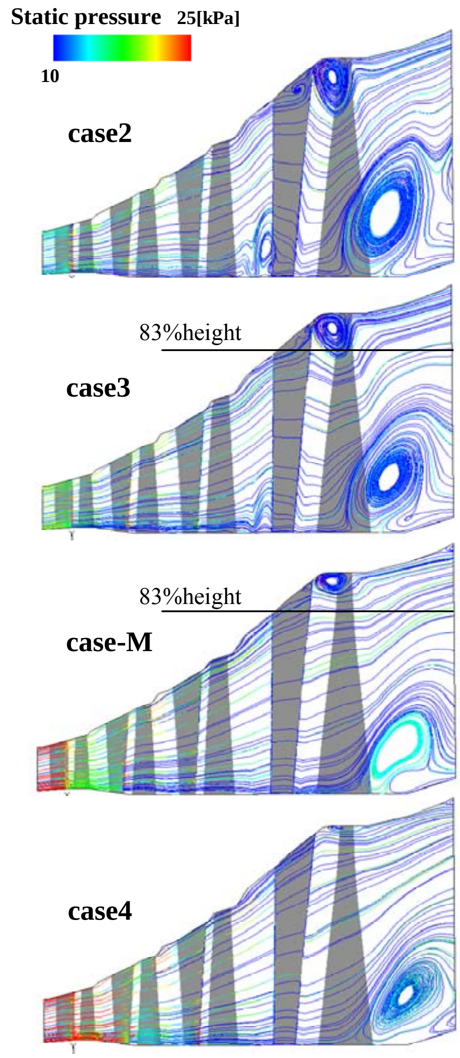

Figure 17 Stream line comparisons in low load conditions

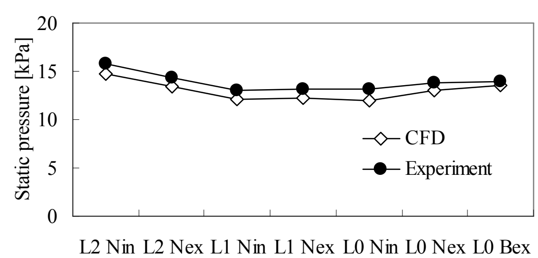

Figure 18 CFD validations by tip end wall pressure comparison

Figure 19 presents the vibration stress trend for various levels of bending stress. It can be seen there are two groups, one of which includes case 2 and case 3, and the other is consists of case M and case 4. These two groups can be provisionally sorted in "with tip reverse flow" and "without tip reverse flow" group, but the data in both groups are so scattered that more distinctive parameter is necessary. Also it is difficult to decide reasonable criteria of “reverse flow”. So, the idea which adopts σ_{bend} should be used only for rough estimation but not enough to understand the physics.

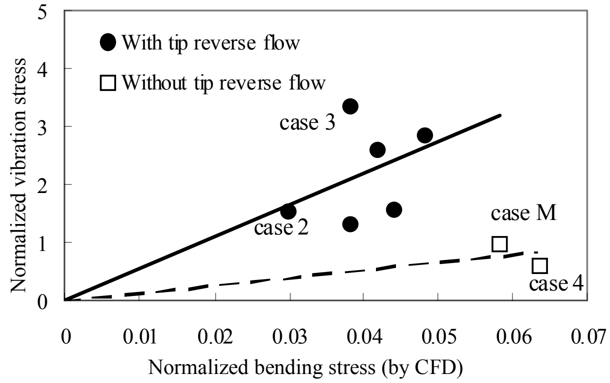

Figure 19 Relationship between measured vibration stresses and calculated bending stresses

Pressure ratio over the L-0 blade tip “PRtip” was investigated in Figure 20, and CFD results present almost same manner against Vax qualitatively. It is considerable that the CFD analysis will give useful information about the flow aspects of tip region. However, it is still difficult to find a sign with which vibration stresses increase. Then, some detailed investigations were also carried out which mainly compared case 3 with case M, where the vibration stress starts to increase.

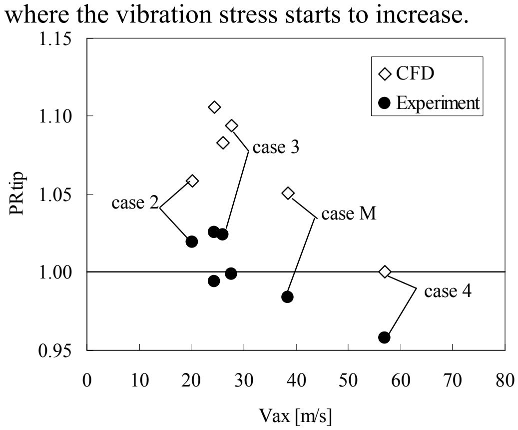

Figure 20 Pressure ratios over the L-0 blade tip by CFD

Radial distributions of dynamic pressure and axial velocity were described in Figure 21. As the stage loading becomes lower, the peak level of dynamic pressure decreases and its radial position goes inward as shown in Figure 21(a), which is consistent to the propagation of circulation shown in Figure 17. And the axial velocity also tends to become smaller and reverse flow region spreads from the tip as shown in Figure 21(b). The combination of these two results in the production of a counter moment against the steam force, because, in the low load condition, the steam flow should push the L-0 blades in an anti-rotational direction which produces negative torque (defined as *Tr* in equation (4)) as shown in Figure 22. From case 4 to case M, the torque goes less at the middle span. Then, from case M to case 3 and case 2, it recovers particularly at about 80% height. As this rapid change of the torque was thought to have much to do with excitation, the blade to blade flow field was precisely examined.

$$T_r = rdr\oint_{bld} p \cdot dx \qquad (4)$$

Figure 23 explains that, in case M, the flow tends to run along the SS and makes a stagnation point near the leading edge (L.E.), while case 3 shows lower velocity because the region is swallowed by the tip large vortex coming downstream. To understand the chaotic flow field, the radial velocity contours were investigated in Figure 24, which revealed that the blade-to-blade path has a strong outward flow region along the P.S. of the blade. The three-dimensional stream constructions shown in Figure 25 explain the physics as follows: The flow coming into the blade row near the hub is obligated to turn outward because of the existence of a huge reverse flow region. Because of the strongly negative inflow, there is a high pressure field along the blade suction side to keep the stream away. Most of the inlet flow then has to move toward the PS, which will create the strong outward flow mentioned above. Only the flow coming from a higher radial position than the reverse flow zone can run downward along the blade SS. The strength of the outward flow seems to something to do with the blade instability.

Figure 26 is a comparison of the blade surface pressure distribution of 83% span. In both cases, surface pressure is higher on the suction side (SS) than on the pressure side (PS) for most part of the surface. And it is interesting that case M has highly pressurized region near leading edge. It can be assumed that blades are retained by the flow even though it is in an irregular manner like a compressor. On the contrary, in case 3, the pressurized region in the front half is diminished and only that of the aft half remains and blades are likely to response to aerodynamic excitation.

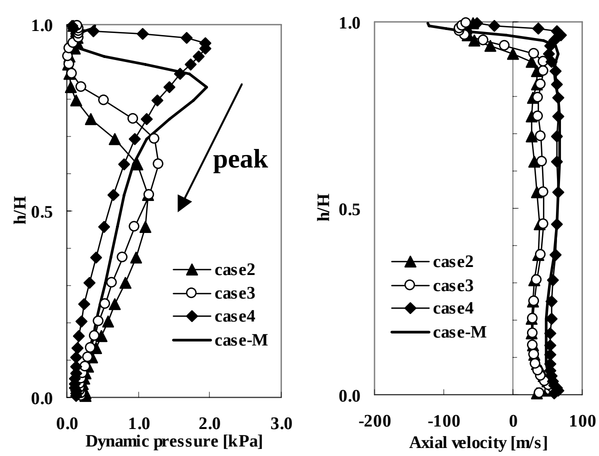

(a) (b)

Figure 21 Radial distribution of (a) relative dynamic pressure, and (b) Axial velocity of L-0 blade inlet by CFD

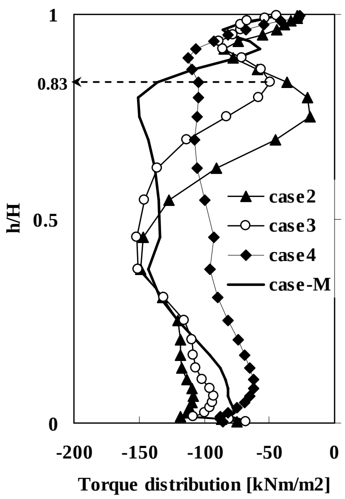

Figure 22 Radial distribution of L-0 blade torque

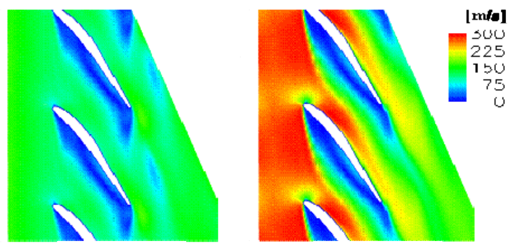

case 3 case M

Figure 23 Velocity contours at 83% height (Radial projection)

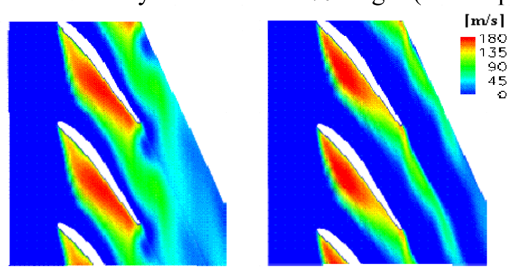

case 3 case M

Figure 24 Radial velocity contours at 83% height

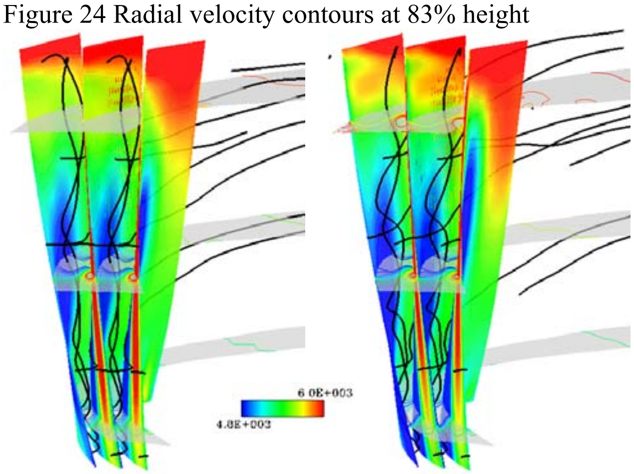

case 3 case M

Figure 25 Flow mechanisms of low load condition and static pressure contours

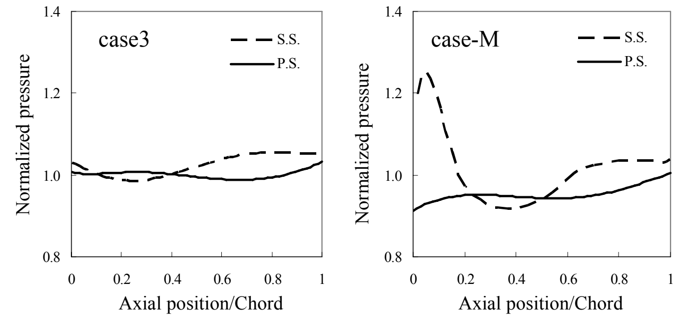

Figure 26 Comparison of blade surface pressure distribution at 83% height

<u>Full arc analyses</u>

Full arc, four stage analyses were performed for case 2, case 3 and case 4 to simulate cyclic fluid force by rotation. Figure 27 shows the axial component of the force distribution. Considerable non-uniformity exists mainly because the number of nozzles and blades are different, and also because the model contains the casing and piping to simulate the test turbine condition as precise as possible. Figure 28 compares the FFT results of the aerodynamic excitation force per unit length on outer 1/3 part of the blade for each case. In addition, measured vibration stresses are overwritten. Note that in this post procedure, the circumferential flow field distribution is thought to be equivalent to unsteadiness.

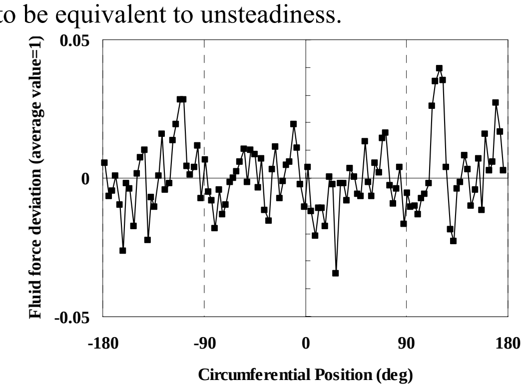

Figure 27 Fluid force distribution of the L-0 blade (the axial component of case 3)

It is interesting that the fluid force of each harmonic order in case 3 is larger than that of other cases, especially in 5th and more order. Particularly, case 4 shows much less excitation force than case 3, despite that it is in higher steady pressure condition as shown in Figure 11. It is also remarkable that there seems to be considerable correlation between the steam force and vibration stress. These variations are considered much to do with the size of blade tip circular region.

In case 2, the peak frequency is at the axial 1st mode and excitation force also has a peak in 4th harmonic, which is closest to axial 1st mode. In case 3, as the stress peak moves to the axial 2nd, 5th and 6th harmonic of the steam force increase to be two or three times as much as those of case 2. Furthermore, the trend of steam force growth in 8th and more harmonics would be in the same manner as the measured wall pressure fluctuation shown in Figure 15, which implies the rotational pressure fluctuation should play a significant part in blade vibration. Even though the natural frequencies are not coincident with any harmonics, rotational fluctuation would be a possible factor to promote a blade resonance.

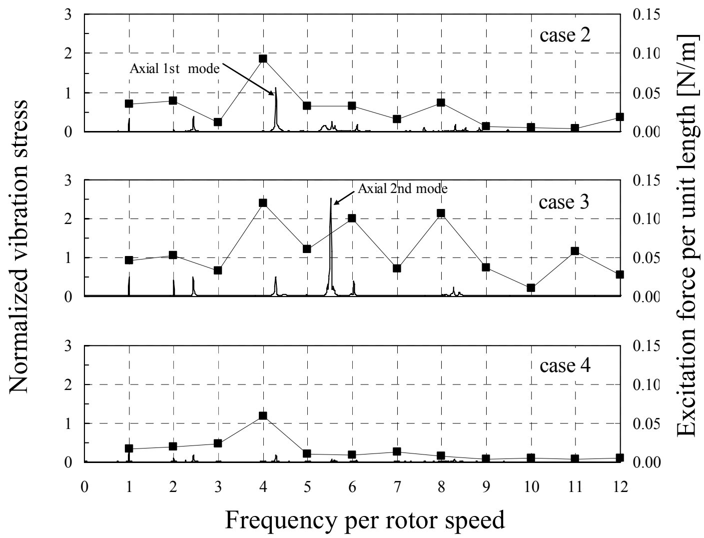

Figure 28 FFT steam force of the tip region and vibration stress of the L-0 blade

CONCLUSIONS

A series of experiments and CFD has been carried out to investigate the correlation between vibration stress behavior, steady pressure and unsteady pressure fluctuation.

It was confirmed that the wall pressure ratio over the L-0 blade tip is a good indicator to predict the vibration stress as Gerschütz et al.[12] suggested.

The result of spectrum analyses of unsteady pressure at the exit of the L-0 nozzle explains that the pressure fluctuation can be an excitation factor, and its frequency depends on the steam condition.

The flow mechanism at very low load conditions was explained by blade-to-blade steady analyses. It can be assumed that blades are retained by the strong anti-rotational flow around leading edge, even though it is in an irregular manner like a compressor. When it is removed by large circular flow, blades are likely to response to aerodynamic excitation.

To estimate the harmonic excitation force, the full arc analyses were carried out. The harmonics which indicate high steam force are correlated with stress peak modes. Even though the natural frequencies are not coincident with any harmonics, rotational fluctuation would be a possible factor to promote a blade resonance.

Note;

Product names mentioned herein may be trademarks of their respective companies.

REFERENCES

[1] K., Ikeuchi, K., Kashiwabara, K., Hisano, K., Namura and A., Uenishi, 1981, "Recent Technology of Long Blade for Steam Turbine," *The Thermal and Nuclear Power, vol. 33, No. 5,* pp. 47-57

[2] K., Iwanaga, H., Kawakami, S., Hisa and H., Ogata, 1985, "Reliability of Last Stage Blade for Steam Turbine under Minimum Load Operation," *The Thermal and Nuclear Power, Vol.36, No.9,* pp.21-34

[3] A., Suzuki, S., Hisa, S., Nagao and H., Ogata, 1986, "Development of 52-inch Last Stage Blade for Large Steam Turbines," *1986 Joint Power Generation Conf.,* 86-JPGC-Pwr-41

[4] Mujezinovic, A., Hofer, D., Barb, K., Kaneko, J., Tanuma, T. and Okuno, K., 2002, "Introduction of 40/48 Inch Steel Steam Turbine Low Pressure Section Stages," *Proceeding of the Power-GEN Asia,* (2002), CD-ROM.

[5] Y., Sugita, K., Sugiyama, T., Kuramoto, T., Matsuura, H., Uchida and K., Kase, 2000, "Blade Vibration and Temperature Measurement in Steam Turbine HP Control Stage and LP Stage," *The Thermal and Nuclear Power, Vol. 51, No. 3,* pp. 26-34

[6] H., Stüer, F., Truckenmüller, D., Borthwick and J. D., Denton, 2005, "Aerodynamic Concept for Very Large Steam Turbine Last Stages," *ASME GT2005-68746*

[7] C., Masuzawa, T., Adachi, E., Watanabe and M., Ishida, 2000, "Computational Analysis and Experimental Verification of Reverse Flow in a Low Pressure Steam Turbine under the Low Load Operation," *Transactions of the Japan Society of Mechanical Engineers, Series B, Vol.66, No.649,* pp. 26-33

[8] E., Saito, Y., Yamashita and T., Kudo, 2009, "Basic Study of Random Vibration for Turbine Blade Structure," *Proc. of the International Conference on Power Engineering-09, Vol. 2,* pp. 511-515

[9] T. Nakamura, N., Iosbe, K., Segawa and T., Saito, 2009, "Highly-reliable Design Technology of Steam Turbine for Nuclear Power Plant," *Hitachi Hyoron, Vol. 91, No. 02,* pp. 224-225

[10] K., Segawa, 2010, "Flow Measurement Technologies Steam Turbines," *Turbomachinery, Vol.38, No.9,* pp. 20-27

[11] F., Truckenmüller, W., Gerschütz, H., Stetter and H.-G., Hosenfeld, 1999, "Examination of the dynamic stress in the moving blades of the last stage in a low-pressure model turbine during windage," *IMechE 1999,* C557/024

[12] W., Gerschütz, M., Casey and F., Truckenmüller, 2005, “Experimental investigations of rotating instabilities in the last stage of a low pressure model steam turbine during windage," *Journal of Power and Energy, September 2005, Vol. 219, No. A6,* pp499-510

[13] R., Sigg, C., Heinz, and M. V., Casey, 2009, “Numerical and experimental investigation of a low pressure steam turbine during windage,” *Proc. IMechE Vol. 223 Part A: J. Power and Energy*, pp. 697-708